ISSN 1063-780X, Plasma Physics Reports, 2023, Vol. 49, No. 4, pp. 403–418. © The Author(s), 2023. This article is an open access publication.
Russian Text © The Author(s), 2023, published in Fizika Plazmy, 2023, Vol. 49, No. 4, pp. 305–321.

TOKAMAKS

Hot Ion Mode in the Globus-M2 Spherical Tokamak

G. S. Kurskiev[a,*], N. V. Sakharov[a], V. K. Gusev[a], V. B. Minaev[a], I. V. Miroshnikov[a], Yu. V. Petrov[a], A. Yu. Telnova[a], N. N. Bakharev[a], E. O. Kiselev[a], N. S. Zhiltsov[a], P. B. Shchegolev[a], I. M. Balachenkov[a], V. I. Varfolomeev[a], A. V. Voronin[a], V. Yu. Goryainov[a], V. V. Dyachenko[a], E. G. Zhilin[b], M. V. Iliasova[a], A. A. Kavin[a], A. N. Konovalov[a], S. V. Krikunov[a], K. M. Lobanov[c], A. D. Melnik[a], A. B. Mineev[c], A. N. Novokhatsky[a], M. I. Patrov[a], A. V. Petrov[a], A. M. Ponomarenko[d], O. M. Skrekel'[a], V. A. Solovei[e], V. V. Solokha[a], E. E. Tkachenko[a], V. A. Tokarev[a], S. Yu. Tolstyakov[a], E. A. Tukhmeneva[a], E. M. Khilkevitch[a], N. A. Khromov[a], F. V. Chernyshev[a], A. E. Shevelev[a], K. D. Shulyat'ev[a], and A. Yu. Yashin[a,d]

[a] *Ioffe Institute, Russian Academy of Sciences, St. Petersburg, 194021 Russia*
[b] *Ioffe Fusion Technology, St. Petersburg, 194021 Russia*
[c] *Efremov Research Institute of Electrophysical Equipment, St. Petersburg, 196641 Russia*
[d] *Peter the Great St. Petersburg Polytechnic University, St. Petersburg, 195251 Russia*
[e] *Konstantinov Petersburg Nuclear Physics Institute, National Research Center "Kurchatov Institute," St. Petersburg, 188300 Russia*
**e-mail: gleb.kurskiev@mail.ioffe.ru*

Received November 30, 2022; revised January 26, 2023; accepted January 27, 2023

Abstract—NBI-assisted plasma heating with one or two injectors of fast neutral atoms was studied at the Globus-M2 spherical tokamak at the toroidal magnetic fields of 0.8–0.9 T and plasma currents of 0.35–0.4 MA. Measurements of the spatial temperature and electron density distributions, performed using the Thomson scattering diagnostics, showed a twofold increase in heating of plasma electrons during the injection of neutral particles with energies of up to 45 keV at the beam power of 0.75 MW, as compared to the ohmic heating regime. Switching on the second additional beam with the particle energy of up to 30 keV and power of up to 0.5 MW resulted in obtaining the hot ion mode in the range of mean plasma densities of $(1.6–10) \times 10^{19}$ m^{-3}. According to the data of active spectroscopy and neutral particle analyzer diagnostics, in the hot zone, the ion temperature reached 4 keV at the plasma density of 8×10^{19} m^{-3}, which is more than 2.5 times higher than the electron temperature.

Keywords: spherical tokamak, plasma, high-power beams of neutral atoms, heating of electrons and ions
DOI: 10.1134/S1063780X23600214

1. INTRODUCTION

The toroidal magnetic field (B_T) highly affects the thermal insulation of plasma in spherical tokamaks (ST). Experiments performed at different facilities with small aspect ratios have shown that an increase in the B_T field results in a considerable increase in the energy confinement time [1–5]. This makes it possible to obtain the regimes with high plasma temperatures and, consequently, with lower collisionalities $\nu^* \sim Z_{\text{eff}} n_e / T^2$ (here, Z_{eff} is the effective charge of plasma ions, T is the volume-averaged plasma temperature, and n_e is the mean plasma density). It has been experimentally established that a decrease in collisionality favorably affects the confinement of plasma energy in STs [5–7]. The reduction of collisionality favorably affects the thermal insulation of electrons in STs since it stabilizes the small-scale instabilities responsible for the electron-associated heat loss: electron temperature gradient instability (ETG) and micro-tearing modes (MTM) [5–7]. At STs, in the regimes with improved confinement (H-mode), the ion temperature gradient instability (ITG), which is the main driver of anomalous ion-associated heat transport, is usually stable [8, 9]. The ion thermal diffusivity determined experimentally is good described by the neoclassical theory [2–5, 7, 10, 11], which also predicts an improvement in the thermal insulation of ions with decreasing collisionality [12].

In 2012, when designing the Globus-M2 spherical tokamak, the predictive simulations were performed of the spatial temperature distributions of electrons and ions in plasma of the facility under design [13]. It was predicted that for a small spherical tokamak with the aspect ratio $A = 1.6$, the minor radius $a = 0.22$ m, and the toroidal magnetic field $B_T = 1$, the hot ion

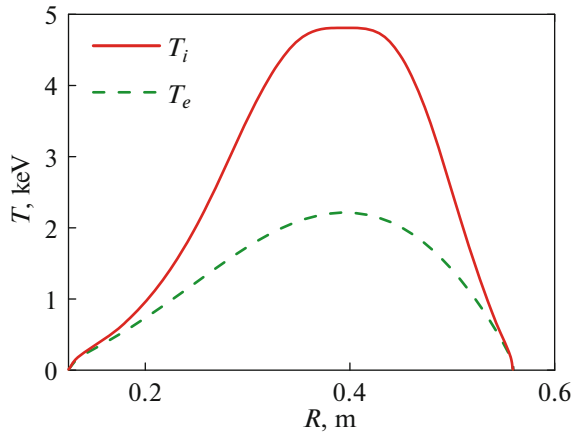

Fig. 1. Temperature profiles of electrons (dashed line) and ions (solid line) in plasma of the Globus-M2 tokamak calculated in 2012 when performing predictive simulations with following parameters: toroidal magnetic field was $B_T = 1$ T; plasma current was $I_p = 0.5$ MA; and deuterium beam with particle energies $E_b = 30$ keV and power $P_{\mathrm{NBI}} = 1$ MW was injected into deuterium plasma.

mode can be obtained, in which the ion temperature (T_i) is 2.5 times higher than the electron temperature, reaching the value of 5 keV (see Fig. 1). It was assumed in the calculations that the plasma current I_p is equal to 0.5 MA, and the deuterium plasma is heated by the injected deuterium beam with the particle energy $E_b =$ 30 keV and power $P_{\mathrm{NBI}} = 1$ MW. In those calculations, the ion thermal diffusivity was assumed to be neoclassical, and the electron thermal diffusivity was set on the assumption that an increase in the energy confinement time, as compared to that obtained at the Globus-M tokamak at $B_T = 0.4$ T, should correspond to the scaling law proposed in [3]. Since the vacuum chambers (and hence the plasma sizes) of the Globus-M2 and Globus-M tokamaks are the same, it was not necessary to take into account the dependence of the characteristic energy confinement time τ_E in plasma on the tokamak size.

In some studies, such successful predictions were questioned. In a number of works, for plasma with small aspect ratio, gyrokinetic modeling was performed of the development of microinstabilities (turbulence). It demonstrated a possible destabilization of the ion temperature gradient instability (ITG) [7, 14, 15] at low collisionalities; this can result in a considerable increase in heat loss through the ion channel. The latter questions the possibility of reaching such high ion temperatures T_i in the compact STs. Additional doubts were caused by the results of experiments at the NSTX spherical tokamak, which revealed the presence of considerable anomalous ion heat transport in low-collisionality regimes [6]. We note that the analysis of first results of the experiments on plasma heating at the Globus-M2 tokamak showed the three-fold excess of the ion thermal diffusivity over the neoclassical one [15]. In these experiments, the additional heating was used by one neutral beam with particle energy of 28 keV and beam power of 0.8 MW at the following facility parameters: the toroidal magnetic field was 0.8 T, the plasma current was 0.4 MA, and the mean plasma density was (6–7) $\times 10^{19}$ m^{-3}. Since the heating pulse duration was limited to 50 ms, the beam was switched on in the phase of current plateau.

The goal of this article is to analyze the results of experiments on plasma heating at the Globus-M2 spherical tokamak using the method of neutral beam injection at the toroidal magnetic fields of 0.8–0.9 T and plasma currents of 0.35–0.4 MA. Putting into operation the new injector of neutral particles with energies up to 45 keV [16] made it possible to provide for plasma heating during the entire facility shot, starting from the phase of current rise. Using the injector [17] previously available at the facility, it is possible to additionally increase the plasma heating power during up to 40 ms in the selected discharge phase. The tokamak is equipped with the new Thomson scattering diagnostic complex, which makes it possible to measure the dynamics of temperature and electron density profiles from the beginning of the shot till its end at 10 spatial points with the pulse repetition rate of 330 Hz (with no limitation on the number of time points). This advances the capabilities of conducting research at the Globus-M2 tokamak. The article is structured as follows. The descriptions of the facility, the neutral beam injection complex, and the main diagnostic systems are given in Section 2. The experiments are considered in Section 3 on plasma heating using single beam with particle energies of up to 45 keV at $B_T = 0.8$ T and $I_p = 0.4$ MA. In Section 4, the hot ion mode is analyzed, obtained in the course of simultaneous heating the plasma with two neutron beam injectors at $B_T = 0.9$ T and $I_p = 0.35$–0.4 MA.

2. THE GLOBUS-M2 TOKAMAK

The studies reported in this work were performed at the Globus-M2 spherical tokamak [13, 18], the major and minor radii of which are $R = 0.36$ m and $a =$ 0.24 m, respectively. The small aspect ratio makes it possible to obtain stable shots with the plasma current of 0.4 MA at the toroidal magnetic fields of 0.8–0.9 T. The planned increase in the toroidal magnetic field, as compared to the design value of 1 T, will make possible the operation at plasma currents of up to 0.5 MA. The magnetic diagnostics makes it possible to determine the location of the last closed magnetic surface of the plasma column using the algorithm of movable current rings [19, 20]. In the facility shots discussed in this work, the magnetic configuration with the lower X-point was created during the current plateau at the plasma elongation of 1.8–2 and triangularity of 0.35–0.4.

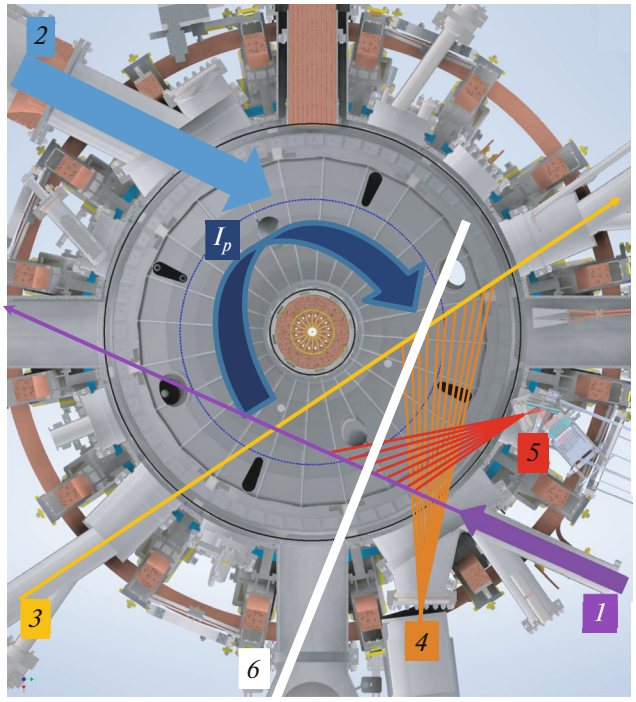

Fig. 2. Equatorial cross section of the Globus-M2 tokamak: (*1*) NI-1 injector of atoms; (*2*) NI-2 injector of atoms; (*3*) laser of Thomson scattering system; (*4*) observation chords of Thomson scattering diagnostics; (*5*) observation chords of CXRS diagnostics; and (*6*) observation chords of longitudinal neutral particle analyzer of charge-exchange atoms. Dashed line shows plasma boundary from low magnetic field side.

The arrangement of the injectors, as well as the main diagnostic systems, is shown in Fig. 2. The impact parameters of both injectors are 30 cm. Both beams are injected tangentially along the plasma current. In the experiments under discussion, the NI-1 tokamak injector [17] was equipped with the IPM-2 ion source, which makes it possible to obtain the beam of hydrogen (deuterium) atoms with energies of up to 30 keV, beam power of up to 0.5 MW and geometric dimensions of approximately 6 × 15 cm [21]. The second NI-2 injector produces the beam of high-energy hydrogen (deuterium) atoms with energies of up to 50 keV, beam power of up to 1 MW, and the diameter of approximately 11 cm.

A number of diagnostic systems was used to study the plasma heating. The diamagnetic flux measurements make it possible to determine the energy stored in the plasma using the PET equilibrium code [22, 23]. The Thomson scattering (TS) diagnostics, completely updated in 2020 [24, 25], provides for measuring the electron temperature and density profiles with the repetition rate of 330 Hz during the entire facility shot from the time of breakdown till the discharge end at ten spatial points located from the plasma boundary to the magnetic axis from the low magnetic field side. The joint analysis of the TS diagnostics data and the results of magnetic equilibrium reconstruction makes it possible to determine the thermal energy of the plasma electron component, as well as the mean electron density during the entire shot. The diagnostics of charge exchange recombination spectroscopy (CXRS) [26, 27] makes it possible to measure the ion temperature at eight spatial points. In the experiments under discussion, time resolution of the CXRS diagnostics was 5 ms. The ion temperature can also be determined using the neutral particle analyzer (NPA) [28]. The NPA observation geometry allows localizing the measurements at the intersection of the analyzer observation line and the injection chord of the NI-1 beam. Unfortunately, the measurements of plasma ion temperature using the CXRS diagnostics and the "active NPA" technique are possible only during the NI-1 injector operation. In addition, in a number of facility shots, neutron fluxes were measured using the SNM-11 corona counter, the principle of operation of which is based on detecting the nuclear reaction of neutrons with the ^{10}B boron isotope placed into the polyethylene moderator. The correlation between the detector counts and the neutron yield from the plasma was found with the help of the in situ calibration performed using the IBN-241 reference neutron source [29].

3. PLASMA HEATING IN THE GLOBUS M2 TOKAMAK USING NEUTRAL BEAM WITH PARTICLE ENERGIES OF 45 keV AT TOROIDAL MAGNETIC FIELD OF 0.8 T

3.1. Experimental Results

A series of experiments on plasma heating was performed using the NI-2 neutral beam with the particle energies of 45 keV and beam power of 0.75 MW. The experiments were performed at the plasma current of 0.4 MA and the toroidal magnetic field of 0.8 T (at the radius R = 0.36 m). Figure 3 shows the dynamics of plasma parameters for several facility shots from this series. The hydrogen beam was switched on in the phase of plasma current rise, and the heating lasted until the end of the current plateau. In the shots, the mean plasma density was varied in the wide range $\langle n_e \rangle = 1 \times 10^{19}$–$7 \times 10^{19}$ m^{-3} by means of changing the deuterium injection scenario. The mean plasma density measured using microwave interferometer was in good agreement with the data obtained using the TS diagnostics before the beginning of the sawtooth oscillations development, the presence of which often makes it difficult to measure the density using the interferometer. The dynamics of the electron temperature at the plasma axis (measured by the TS diagnostics) is also shown in Fig. 3. It can be seen that the electron temperature weakly depends on the mean plasma density, reaching the value of 1.3 keV. For shots with different densities, the spatial distributions of

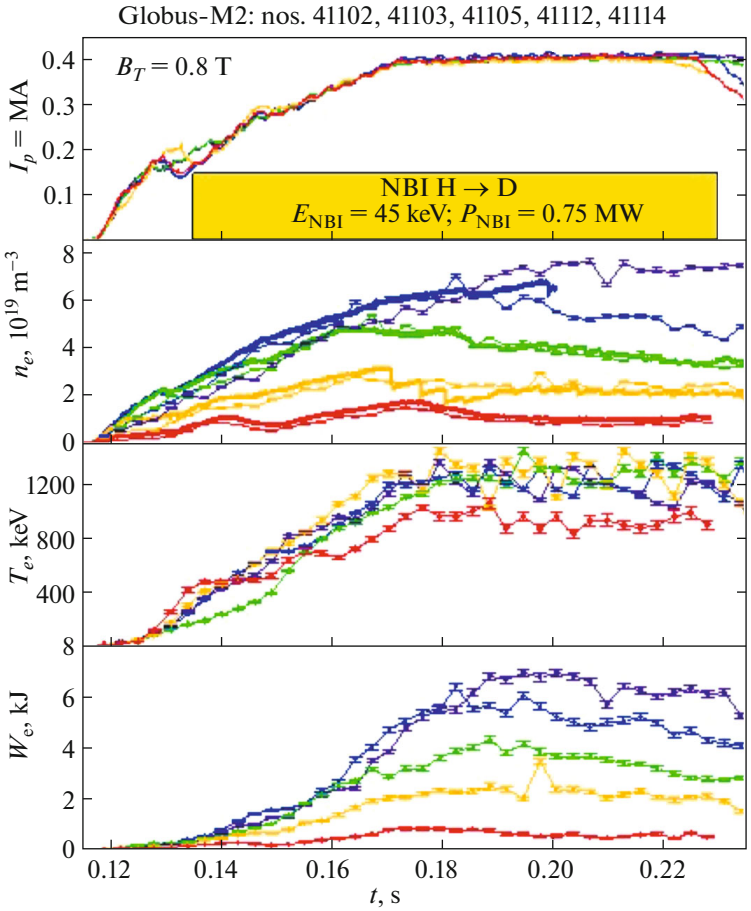

Fig. 3. Time evolution of plasma parameters in experiments on injection of neutral particles with energies of 45 keV and bean power of 0.75 MW at toroidal magnetic field of 0.8 T. From top to bottom: I_p is plasma current (operating time of neutral beam is shown in yellow); n_e is chord-averaged plasma density (lines and dots correspond to data of microwave interferometer and results of processing data of the Thomson scattering diagnostics and magnetic reconstruction, respectively); T_e is electron temperature at the plasma axis (data of the Thomson scattering diagnostics); and W_e is thermal energy of electrons calculated based on data of the Thomson scattering diagnostics and magnetic reconstruction.

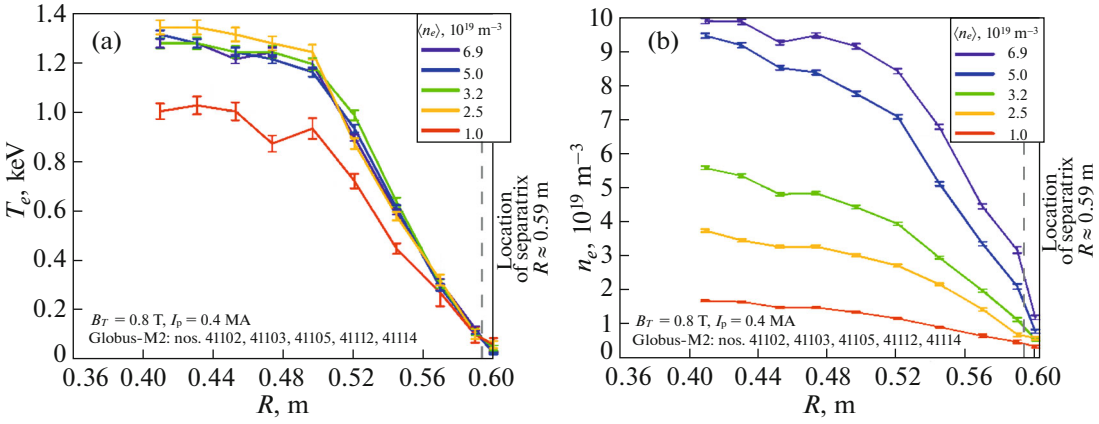

Fig. 4. Spatial distributions of (a) T_e temperature and (b) n_e electron density during injection of neutral particles with energies of 45 keV, beam power of 0.75 MW, plasma current of 0.4 MA and toroidal magnetic field of 0.8 T.

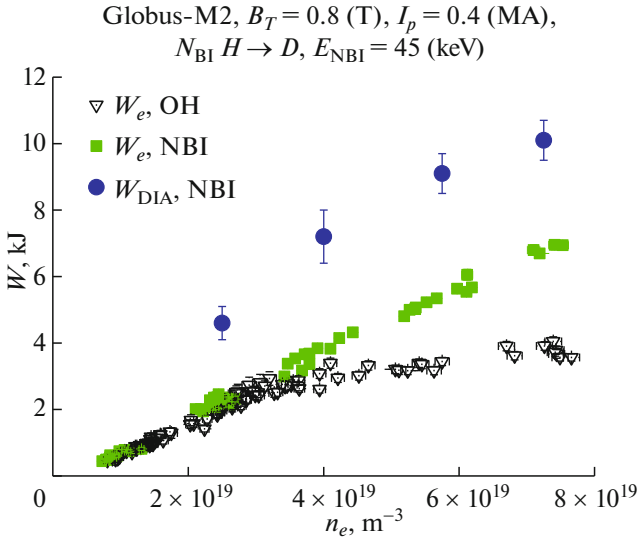

Fig. 5. Thermal energy of electrons W_e as a function of mean plasma density n_e for ohmic heating regime (OH) and regime with injection of neutral particles (NBI) with energies of 45 keV and beam power of 0.75 MW at the same plasma current (0.4 MA) and toroidal magnetic field (0.8 T).

electron temperature and density are compared in Fig. 4. With an increase in the mean electron density $\langle n_e \rangle$, a sharp density gradient is formed near the separatrix that indicates that the plasma is in the improved confinement mode (H-mode). The electron temperature gradient almost does not change outside the convective zone of the sawtooth oscillations development $r/a \approx 0.4$, which corresponds to the region $R > 0.49$ m in the figure.

In the shots with higher density, the electron thermal energy (W_e) obtained by integrating the electron pressure profile over the plasma volume is higher. For the shots under consideration, Fig. 5 shows the W_e energies as functions of the mean plasma density in comparison with those obtained in a series of shots with ohmic heating (OH) at the same plasma current and toroidal magnetic field: $I_p = 0.4$ MA and $B_T = 0.8$ T. In this figure, it can be also seen that at the mean electron densities higher than 3×10^{19} m^{-3}, the neutral beam injection results in considerable heating of plasma electrons. According to the data of the Thomson scattering diagnostics, the electron temperature is almost independent of the density. The thermal energy of electrons increases linearly with increasing density, while in the OH regime (at the same I_p and B_T parameters), the electron temperature decreases with increasing density, which results in saturation of the $W_e(\langle n_e \rangle)$ dependence. The spatial distributions of electron temperature and density in the OH and NBI regimes are compared in Fig. 6 at the mean electron density of 7×10^{19} m^{-3}. It can be seen in the figure that, in the NBI regime, in the paraxial plasma region, the electron temperature is more than twice as high as that in the OH regime, while the thermal energy of the electron component increases by 1.8 times.

For the NBI regime, the stored plasma energy W_{DIA} determined from diamagnetic measurements is also shown in Fig. 5. In the entire range of plasma density variation, the W_{DIA} energy is 1.5–2 times higher than the W_e energy stored in the plasma electron component in the OH regime. The maximum W_{DIA} energy of 10 kJ is reached at the average density $\langle n_e \rangle = 7 \times 10^{19}$ m^{-3}. This is in good agreement with the results previously obtained at the Globus-M2 tokamak in experiments [15, 30], in which the NI-1 injector beam was used to heat the plasma (the particle energy was 30 keV and the beam power was 0.85 MW). The energy stored in the ion component will be discussed below in Subsection 3.2.

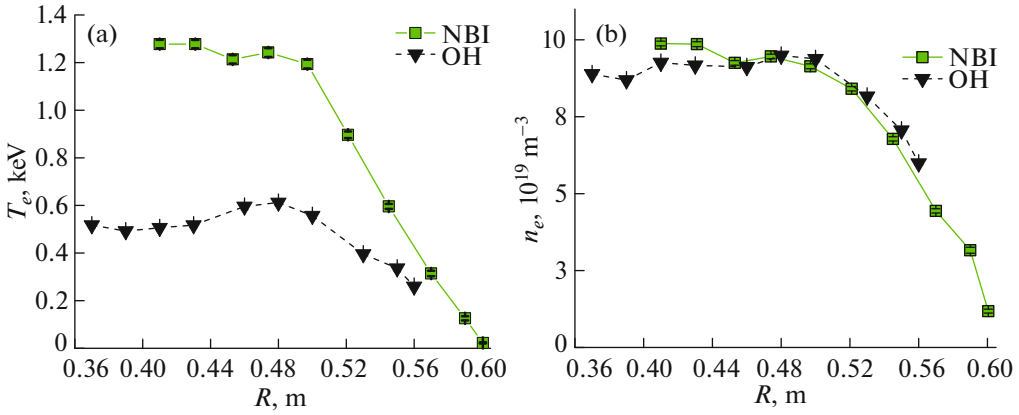

Fig. 6. Comparison of spatial distributions of (a) T_e temperature and (b) n_e density of plasma electrons in OH regime (black triangles) and regime with additional NBI heating (green squares) at plasma current $I_p = 0.4$ MA and toroidal magnetic field $B_T = 0.8$ T.

3.2. Calculations of Absorbed Heating Power

To determine the characteristic time of plasma energy confinement and analyze the energy transport, it is necessary to know the absorbed power of the injected neutral beam. The NUBEAM code [31] was used to calculate the spatial distributions of powers spent on the heating of plasma electrons and ions, as well as the W_{fast} energy corresponding to the transverse pressure of fast particles. We note that in calculations, the loss of fast particles from plasma of the Globus-M2 tokamak due to the magnetic field rippling was not taken into account, since it is negligibly small, as compared to that due to other loss mechanisms. The first studies of the effect of field rippling on the loss of fast ions were performed at the Globus-M tokamak using the ray-tracing code [32]; the rippling amplitude was taken to be ~1.5% at the outer vacuum chamber wall. Calculations have shown that this loss do not exceed several fractions of a percent of the total injected neutral beam power. At the Globus-M2 tokamak, the particle loss due to the field rippling is even less, since the outer coils of the toroidal winding are moved outward by 4 cm farther [18], as compared to the Globus-M tokamak, and the field rippling is approximately 2 times lower. The sawtooth oscillations more strongly affect the confinement of fast particles. In simulations, to take into account the effect of the sawtooth oscillations on the parameters calculated, the correction was introduced in the form of anomalous additive to the diffusion coefficients of fast particles. Since during the injection of hydrogen, neutron measurements are impossible, the only way available at the Globus-M2 tokamak to experimentally determine the anomalous diffusion of high-energy ions is to compare the calculated and experimental spectra of charge-exchange atoms. The level of anomalous diffusion is iteratively selected in such a way that the calculated spectrum of charge exchange atoms coincides with the spectrum measured using the AKORD-24M longitudinal neutral particle analyzer. The spectra were calculated using the FIDASIM code [33], which involves the distribution of high-energy ions, obtained using the NUBEAM code. The approach used is illustrated in Fig. 7. Here, dots show the signal of neutral particle analyzer recording charge-exchange atoms when the deuterium beam with energy of 45 keV was injected during the sawtooth oscillations (the energy limit of NPA measurements is 35 keV), and the line shows the result of calculations using the NUBEAM and FIDASIM codes. As a result of iterative selection, it was found that the correct description of experimental data requires the introduction of anomalous diffusion. In this case, the anomalous diffusion manifests itself in an increase in the diffusion coefficient of fast ions by 1 m^2/s in the plasma region corresponding to the mixing zone arising due to the reconnection of magnetic field lines during the development of the sawtooth oscillations. The resulting spectrum of charge-exchange atoms (blue line) agrees well with the experimental one. For the anomalous diffusion coefficient of fast ions chosen in this way, the spatial distributions were obtained of the power spent on heating plasma electrons and ions during neutral beam injection; these distributions were used afterwards in transport simulations using the ASTRA code [34]. The integrated absorbed powers of neutral beam, as well as the corresponding W_{fast} energies of fast ions, are presented in Table 1. Using the W_{fast} energies obtained, one can determine the W_i thermal energy of plasma ions as follows: $W_i = W_{DIA} - W_e - W_{fast}$ (see Fig. 8a). The obtained W_i energies are 2.5 times lower than the thermal energies of electrons; apparently, this is a consequence of the corresponding difference between the electron and ion temperatures. As can be seen from Table 1, with increasing plasma density, the power of ions heating by neutral beam also increases, and the power of ions heating in collisions with electrons

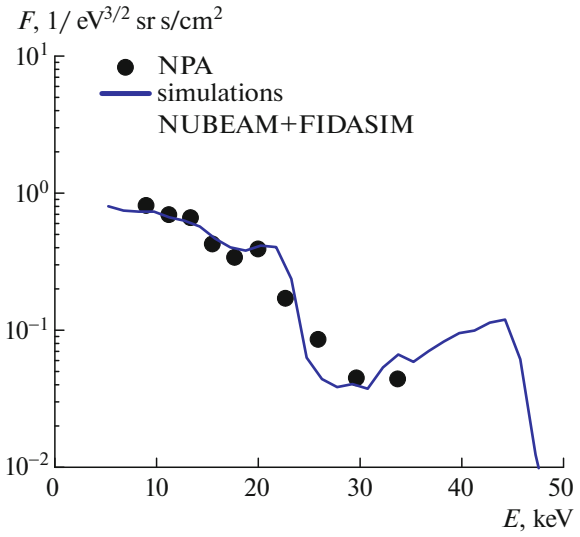

Fig. 7. Spectra of charge-exchange atoms: experimental spectrum (black dots) and spectrum calculated with allowance for anomalous diffusion (blue curve).

Table 1. Integrated absorbed beam powers and pressures of fast particles calculated using the NUBEAM code in shots with different plasma densities. Energy of injected particles is 45 keV, beam power is 0.75 MW, and plasma current and magnetic field are 0.4 MA and 0.8 T, respectively

No.	**41103**	**41112**	**41114**	**41105**
$\langle n_e \rangle$, 10^{19} m^{-3}	**2.5**	**4.0**	**5.8**	**7.3**
$Pnbi_e$, kW	174	230	262	282
$Pnbi_i$, kW	197	256	266	269
$Pnbi_{tot}$, kW	372	486	528	550
W_{fast}, J	1940	1414	1183	920

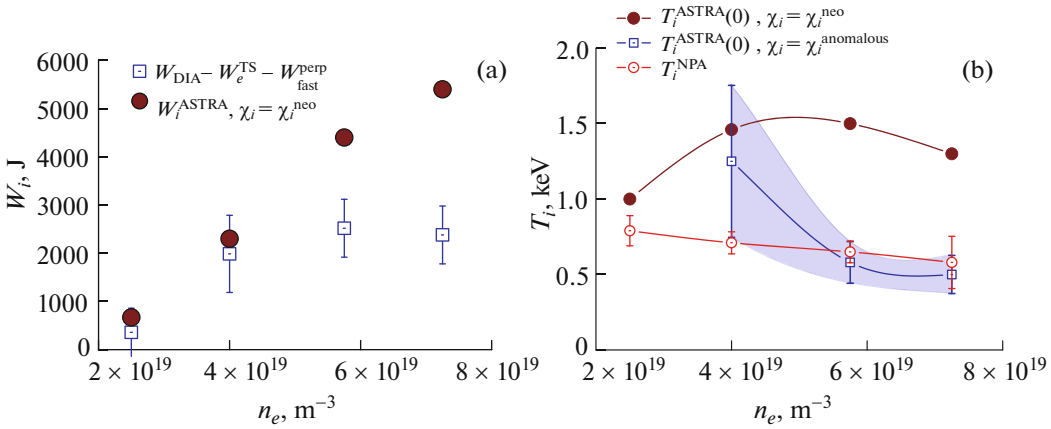

Fig. 8. Thermal energy of ions and ion temperature as functions of electron density during injection of neutral particles with energies of 45 keV at beam power of 0.75 MW, plasma current of 0.4 MA, and toroidal magnetic field of 0.8 T. (a) Thermal energy stored by plasma ions: blue open squares correspond to estimate based on experimental data, $W_i = W_{DIA} - W_e - W_{fast}$; solid circles are results of simulations using ASTRA code under assumption $\chi_i = \chi_i^{neo}$; and (b) comparison of ion temperature measured by neutral particle analyzer (red open circles) with results of simulations using ASTRA code for $\chi_i = \chi_i^{neo}$ (solid circles), and with allowance for anomalous additive for χ_i (blue open squares).

should increase as well. This means that the saturation of the dependence of thermal ions energy on plasma density observed with increasing density is an indicator of deterioration in the thermal insulation of ions.

3.3. Simulations of Plasma Energy Balance

The following model was used when analyzing the energy transport in the Globus-M2 tokamak plasma with the help of the ASTRA code. In simulations, the energy balance equation for ions (without the convection term) was solved along with the diffusion equation for the poloidal magnetic flux and the Grad–Shafranov equation. As a boundary condition for the Grad–Shafranov equation, the boundary of the last closed magnetic surface was set, which was obtained using the method of movable current rings. To calculate the density of deuterium ions, the electrical resistance of the plasma, and, as a consequence, the OH power, we used the effective charges of the plasma obtained from measurements of the bremsstrahlung intensity [35]. For the shots under consideration, the effective charges measured are presented in Fig. 9. Carbon was specified as the main impurity, since the plasma-facing surface is covered with graphite plates. Using the NCLASS code [36], the plasma conductivity and the fraction of bootstrap current were calculated, as well as the neoclassical coefficients of ion thermal diffusivity (χ_i^{neo}) (see the solid lines in Fig. 10a); at the plasma densities higher than 5×10^{19} m^{-3}, the χ_i^{neo} coefficients turn out to be in the range of 0.8–1.5 m^2 s^{-1}. The ion temperatures (according to the ASTRA code), as well as the thermal energies of the ion component, obtained in simulations under the assumption $\chi_i = \chi_i^{neo}$, are shown in Fig. 8. It can be seen in the figure that in the case of neoclassical heat transport through the ion channel, the thermal energies W_i stored by ions should be much higher than the experimentally measured ones, and in the paraxial plasma region, the ion temperature should become close to (but not higher than) the electron temperature (~1.2–1.3 keV). In order to bring the calculated W_i energies in line with the experimentally

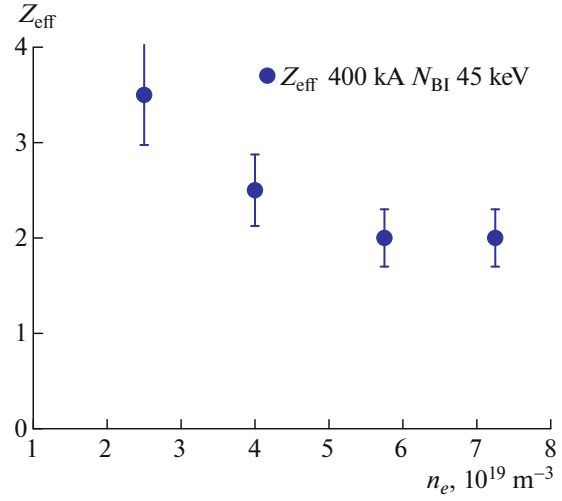

Fig. 9. Effective plasma charge Z_{eff} measured in a series of shots with injection of neutral particles with energies of 45 keV at beam power of 0.75 MW, plasma current of 0.4 MA and toroidal magnetic field of 0.8 T.

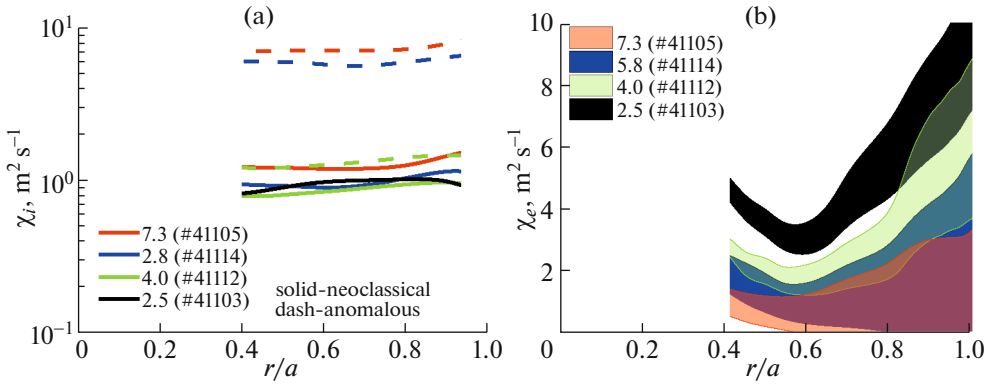

Fig. 10. Spatial distributions. (a) Thermal diffusivity of ions χ_i used in calculations of ion temperature profiles; solid and dashed lines correspond to neoclassical calculations and thermal diffusivities fitted based on magnetic measurements, respectively. (b) Thermal diffusivity of electrons χ_e obtained in simulations using ASTRA code based on electron temperature profiles measured experimentally. Simulations were performed for shots with different densities (corresponding mean densities are shown in insert in units of 10^{19} m^{-3}) during injection of hydrogen atoms with energies of 45 keV at beam power of 0.75 MW, plasma current of 0.4 MA and toroidal magnetic field of 0.8 T.

measured ones, the additional calculations were performed, in which the anomalous additive was added to the neoclassical thermal diffusivity χ_i^{neo}. The anomalous additive was determined iteratively by comparing the calculated energy of plasma ions with the experimental estimate. The obtained anomalous ion thermal diffusivities are 5–6 times higher than the neoclassical ones (see dashed lines in Fig. 10a). The calculated ion temperatures at the plasma axis also turned out to be close to the ion temperatures measured by the neutral particle analyzer (see Fig. 8b).

For the electron plasma component, the inverse transport problem was solved: based on the measured spatial electron temperature distributions, the χ_e coefficients of electron thermal diffusivity were calculated (see Fig. 10b). Unfortunately, in the shots under discussion, the energy loss due to plasma emission was not measured. As shown by previous studies performed at the Globus-M2 tokamak, in the regimes with NBI, the radiation loss can reach 45% of the total heating power absorbed in plasma [37]. Therefore, to take into account the effect of radiation loss on the χ_e coefficient, the calculations were performed with allowance for the radiation loss, in which the corresponding profile was used taken from [37]. For each of the regimes, the profile was normalized to the integrated radiation loss power obtained by multiplying the power absorbed in the plasma by the empirical coefficient of 0.45. In addition, the χ_e coefficient was calculated without taking into account the radiation loss. Thus, as a result of these calculations, we can assume that the true values of the χ_e coefficient will be in the range between these values (see Fig. 10b and the regions filled with different colors for different plasma densities).

For all the cases that have been under consideration above, the estimates of the energy confinement times are shown in Fig. 11. It can be seen in the figure that the energy confinement time obtained under the assumption of neoclassical nature of heat loss through the ion channel should depend linearly on the plasma density and reach a characteristic time of 15 ms at the plasma density of 7×10^{19} m^{-3} (see green circles in Fig. 11). We analyzed the data of diamagnetic measurements and calculations of the stored plasma energy, along with the results of measuring the electron temperature and density profiles using the Thomson scattering technique. This analysis indicates the

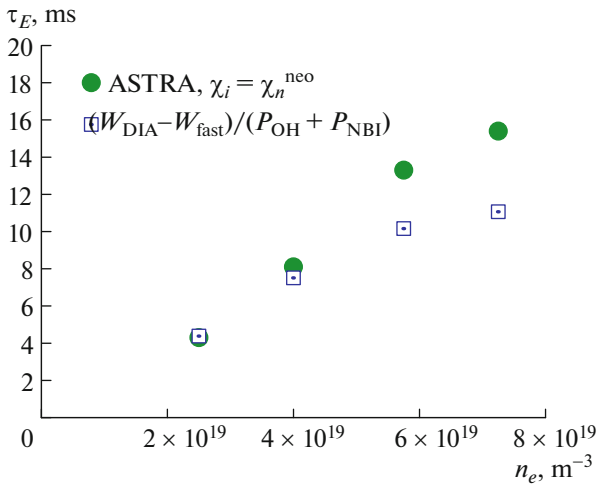

Fig. 11. Energy confinement time τ_E as a function of electron density for a series of shots with injection of neutral particles with energies of 45 keV at beam power of 0.75 MW, plasma current of 0.4 MA and toroidal magnetic field of 0.8 T.

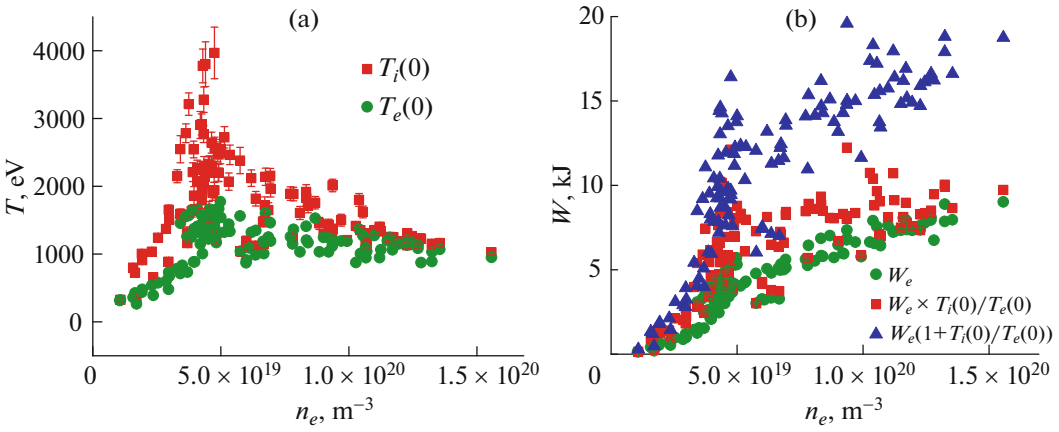

Fig. 12. (a) Electron T_e and ion T_i temperatures (green circles and red squares, respectively) at axis of plasma column as functions of electron density in regimes with simultaneous injection of NI-1 and NI-2 beams at $B_T = 0.9$ T and $I_p = 0.35$–0.4 MA; and (b) corresponding thermal energies W_e stored by plasma electrons (green circles). They were calculated by means of integrating electron pressure over plasma volume and using data of magnetic reconstruction. There are also estimates of thermal energies stored by plasma ions $W_i \approx W_e \times Ti(0)/T_e(0)$ (red squares) and sum of energies stored by both plasma electrons and ions (blue triangles).

presence of anomalous heat loss through the ion channel, which can be the reason for the saturation of the dependence of the τ_E characteristic energy confinement time on the n_e density observed at plasma densities higher than 6×10^{19} m^{-3}. The experiments performed using the new NI-2 injector and the new Thomson scattering diagnostics confirm the results previously obtained at the Globus-M2 tokamak [15, 30]. First, after increasing the plasma current to 0.4 MA and the toroidal magnetic field to 0.8 T, we obtained an increase in the energy confinement time by a factor of 2.5–3, as compared to the experiments performed at $B_T = 0.4$ T. Second, in this case, the electron thermal diffusivity decreases to 1–2 m^2 s^{-1}, which makes it possible to heat plasma electrons to the temperature of 1.3 keV. Third, the estimates of ion temperature based on the diamagnetic measurements and measurements of the NPA diagnostics show that the ion temperature is less than the electron one, $T_i < T_e$, which is due to the fact that the heat transport through the ion channel is higher than that predicted by the neoclassical theory.

4. FIRST EXPERIMENTS ON PLASMA HEATING BY TWO NEUTRAL BEAMS IN THE GLOBUS-M2 SPHERICAL TOKAMAK AT MAGNETIC FIELD OF 0.9 T

4.1. Experimental Results

The experiments (presented in Section 3) performed at the Globus-M2 tokamak using the new injector that makes it possible to introduce the beam of neutral particles with energies up to 45 keV into the plasma demonstrated high efficiency of heating plasma electrons. The analysis of diamagnetic measurements, along with the data of the Thomson scattering diagnostics, demonstrated the low efficiency of ion heating. Apparently, this is associated with high anomalous heat loss through the ion channel, which results in the effect of "saturation" of the dependence of the energy confinement time on the plasma density.

The following scheme for plasma heating was used. The NI-2 beam (with the particle energy of up to 45 keV and power of up to 0.75 MW) was switched on in the stage of current rise, and the NI-1 beam (with the particle energy of up to 28 keV and power of up to 0.45 MW) was switched on already in the stage of current plateau. In experiments on plasma heating using two beams simultaneously, it became possible to measure the ion temperature profile using the CXRS diagnostics. The experiments were performed in deuterium plasma at the toroidal magnetic field of 0.9 T and the plasma current in the range of 0.35–0.4 MA. At the axis of the plasma column, the electron and ion temperatures measured by the TS and CXRS diagnostics during operation of both injectors as functions of the mean plasma density are shown in Fig. 12a. It can be seen in the figure that, in a wide range of the mean plasma densities, the ion temperature considerably exceeds the electron temperature. In this case, with an increase in the plasma density, the ion temperature also increases and reaches its maximum $T_i(0) \approx 4$ keV at the axis of the plasma column at the mean electron density of approximately 5×10^{19} m^{-3}. With a further increase in the plasma density, the ion temperature decreases and becomes close to the electron temperature. It is rather easy to determine the energy stored by thermal electrons by means of integrating over the plasma volume the electron temperature and density profiles measured using the Thomson scattering diag-

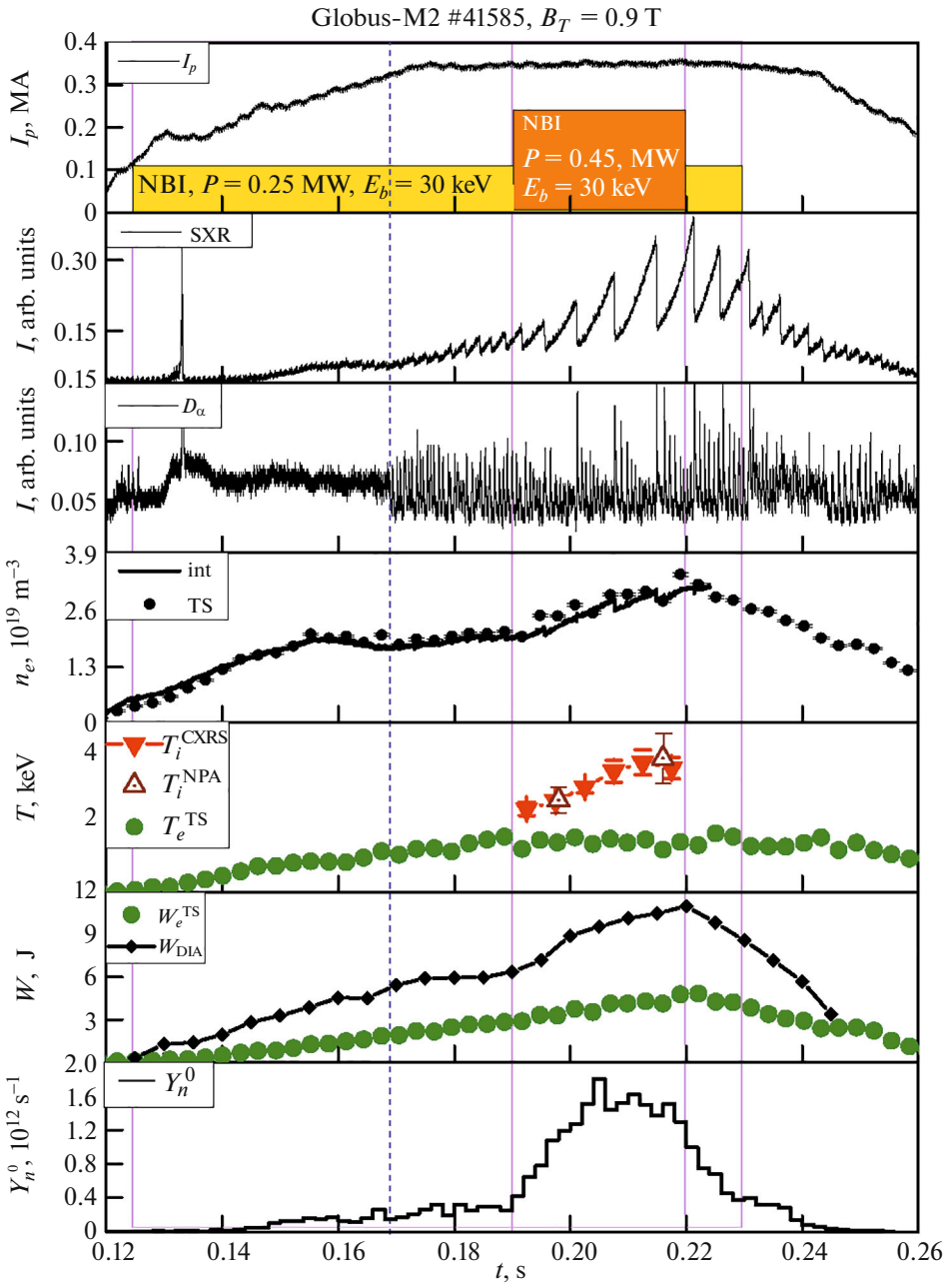

Fig. 13. Time evolution of plasma parameters in shot #41585. From top to bottom: I_p is plasma current; I(SXR) is intensity of soft X-ray radiation; $I(D_\alpha)$ is intensity of $D\alpha$ line of deuterium atoms; n_e is electron density averaged along observation chord; T is temperature of electrons (green circles, Thomson scattering diagnostrics) or ions (open and red triangles correspond to NPA and CXRS diagnostics, respectively); W is plasma energy (black dots, diamagnetic measurements) and energy stored in electron component calculated based on data of Thomson scattering diagnostics (green circles); and Y_n^0 is neutron yield.

nostics (see Fig. 12b). To determine the thermal energy stored in the ion component, the more complicated calculations are required, which take into account that a certain fraction of the main ions is replaced by impurity ions. The energy stored in the ion component can be roughly estimated from above as follows: $W_i \approx W_e \times T_i(0)/T_e(0)$. It can be seen in the figure that the W_e energy monotonically increases with increasing plasma density, and at densities higher than 5×10^{19} m^{-3}, the dependence of the W_i energy on the plasma density begins saturating, which is a consequence of a decrease in the ion temperature with an increase in plasma density.

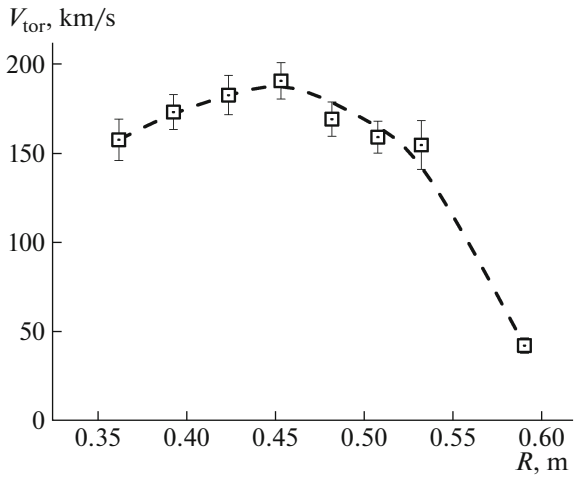

Fig. 14. Toroidal rotation velocity of carbon ions in plasma column as a function of major radius R. Measurements were performed using CXRS diagnostics in shot #41585 at $T_i(0) = 4$ keV.

Let us consider the hot ion mode in more detail by way of example of the shot with the plasma current of 0.35 MA and the mean plasma density of 5×10^{19} m^{-3} (see Fig. 13). The first neutral beam with the power of 0.25 MW was switched on in the stage of plasma current rise. With increasing plasma current, the total power flux through the plasma boundary increased as well. This results in the occurrence of L–H transition at time $t = 169$ ms. The transition is clearly identified by a sharp decrease in the D_α line intensity and the development of the edge-localized instability of the ELM type, which indicates an increase in the steepness of the pressure gradient near the plasma boundary. The second neutral beam with the power of 0.45 MW was injected in the stage of plasma current plateau, which resulted in a strong increase in the ion temperature and, consequently, in an increase in the energy stored in the plasma. The neutron flux recorded by the counter increases by a factor of seven and begins to decrease immediately after the beam is switched off. The neutron yield reaches 1.8×10^{12} neutrons/s. This is the lower estimate, since for calibrating the diagnostics, the Am–Be source was used with the average neutron energy of 4 MeV, which exceeds the energy of neutrons produced in the course of the D–D reaction (2.45 MeV). The ion temperature measured by the CXRS diagnostics using the emission line of fivefold-ionized impurity carbon ion C^{5+} (the emission wavelength is $\lambda_0 = 5290.525$ Å) is in good agreement with the data of active NPA diagnostics, the measurements of which are localized in the region of beam intersection with the NPA observation line. Both diagnostics demonstrate an increase in the ion temperature up to 4 keV during the injection of the second beam. The CXRS diagnostics also shows that due to the neutral beam injection, the plasma acquires the considerable rotational moment: in the paraxial region, the velocity of plasma toroidal rotation reaches 190 km/s (see Fig. 14). The electron temperature at the plasma axis, measured by the Thomson scattering diagnostics, almost does not change; it remains at a level of 1.5 keV during the entire period of the second beam injection, while the plasma density considerably increases. The electron and ion temperature profiles are shown in Fig. 15, as well as the electron density profile measured in shot #41585 at ten spatial points in the median plane of the tokamak.

The W_e and W_i thermal energies of electrons and ions, respectively, were determined by means of integrating the corresponding pressure profiles over the plasma volume. Ions contain most of the plasma

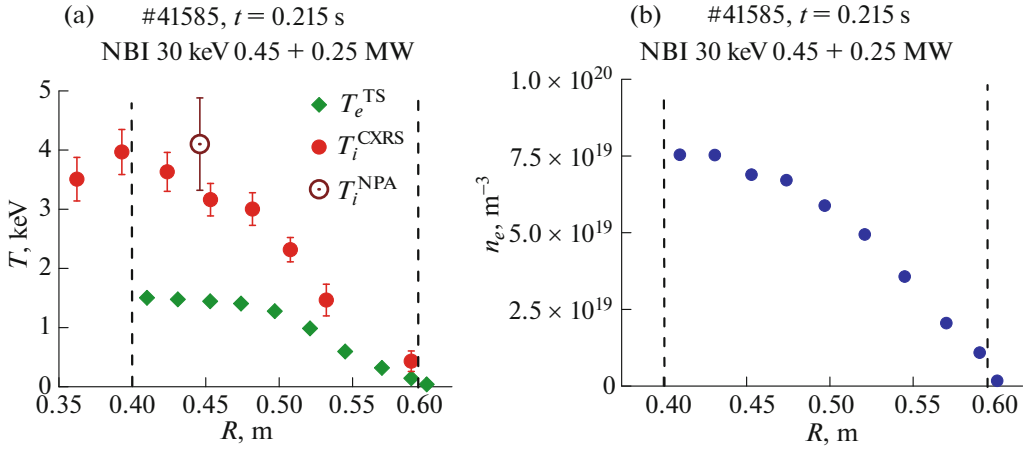

Fig. 15. (a) Spatial distributions of electron and ion temperatures and (b) electron density profile measured at the 215th ms in shot #41585 at $B_T = 0.9$ T and $I_p = 0.35$ MA. Vertical lines mark locations of magnetic axis (left) and last closed magnetic surface from the low magnetic field side (right).

energy (6 kJ). The fraction of energy attributable to electrons is approximately 4 kJ. The total energy determined from diamagnetic measurements based on calculating the magnetic equilibrium reaches 11.5 kJ, which is in good agreement with the data of kinetic measurements, with allowance for the fact that the contribution of the transverse energy of fast ions can be 1.5 kJ.

It is noteworthy that the hot ion mode was predicted when performing simulations of the energy balance in the Globus-M2 plasma; this simulations were performed in 2012 [13] in the stage of designing the electromagnetic system of the future tokamak. The calculated temperature profiles of electrons and ions obtained in [13] are shown in Fig. 1. We note that the predictive simulations were performed at slightly higher toroidal magnetic fields and plasma currents than those in the experiments described. Despite this, the hot ion mode was observed at the T_i and T_e temperatures very close to those predicted. The main assumptions used in predictive simulations were also confirmed. As compared to the results of experiments at the Globus-M tokamak, the ion thermal diffusivity considerably decreased (by ~4 times) in accordance with the neoclassical theory. When the toroidal magnetic field and current increase twice, the plasma energy confinement time increased by a factor of four, which is in good agreement with the scaling laws typical for the spherical tokamaks, which assume the strong dependence of the plasma energy confinement time τ_E on the toroidal magnetic field B_T [2, 5].

4.2. Simulations of Plasma Energy Balance in Hot Ion Mode

To determine the power of plasma heating by neutral beams, the simulations were performed using the NUBEAM code [31]. The oscillogram of the soft X-ray intensity (Fig. 13) indicates the presence of the sawtooth oscillations in the plasma. Regular reconnections of the magnetic surfaces in the paraxial plasma region, that cause of the development of the sawtooth oscillations, result in the redistribution of fast ions over the cross section of the plasma column. In turn, this can result in the additional loss of fast particles and, consequently, in a decrease in the power of plasma heating. In these experiments, the NPA was adjusted to measure the ion temperature, which makes impossible the detection of the suprathermal part of the spectrum. Since that, the method for determining the loss of fast particles during deceleration consisting in comparing the calculated spectra with the experimentally measured ones could not be used. Therefore, a series of calculations was performed at different χ_{fi}^{an} coefficients of the anomalous diffusion of fast ions. The power of ion heating, as well as the total power of heating electrons and ions by neutral beams, as functions of the χ_{fi}^{an} coefficient are shown in Fig. 16. The

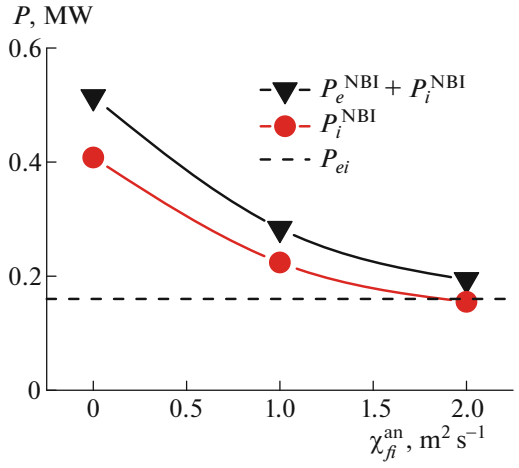

Fig. 16. Power of plasma heating by neutral beams calculated using NUBEAM code in shot #41585 at different coefficients of anomalous diffusion of fast ions: red circles and black triangles correspond to power of ion heating and total power of heating electrons and ions by neutral beam, respectively. Horizontal line shows level of ion heat loss due to interaction with cold electrons.

figure also shows the power of ion heat loss due to interaction with electrons. It can be seen in Fig. 16 that at high levels of fast particle loss, the total power of ion heating turns out to be negative. Further analysis will be performed for two cases. (1) We completely neglect a decrease in the absorbed heating power occurring due to the sawtooth oscillations, and (2) the coefficient of anomalous diffusion of fast particles is assumed to be 1 m^2 s^{-1}. Then we will compare the results for cases (1) and (2). Thus, limiting the power of plasma heating due to the injected beams to the range P_{NBI} = 0.28–0.51 MW, we will obtain the following estimate for the energy confinement time: τ_E = 13–18 ms.

Electrons are heated due to both ohmic heating (P_{OH} = 0.27 MW) and their interaction with thermal plasma ions. The total power of electron heating is in the range of P_e = 0.55–0.78 MW. Ions are heated only by beams and, with allowance for the fact that 0.16 MW of the beam powers is spent on the electron heating, the power of ion heating is in the range of P_i = 0.07–0.25 MW. To roughly estimate the effective coefficient of heat conduction of ions, we can use the following known correlation between the energy confinement time τ_E and thermal diffusivity: $\chi = \rho^2/(4\tau_E)$, where ρ is the radius of the plasma column. Taking $\rho = a\kappa^{0.5}$ and $\tau = W_i/P_i$ (κ is the elongation of the plasma column), we can obtain $\chi_i = a^2\kappa P_i/(4W_i)$. Using this formula, we can obtain the following estimate for the average thermal diffusivity of ions: $\chi_i \approx$ 0.3–1 m^2 s^{-1}. Similarly, we can estimate the electron thermal diffusivity. In this case, the main uncertainty

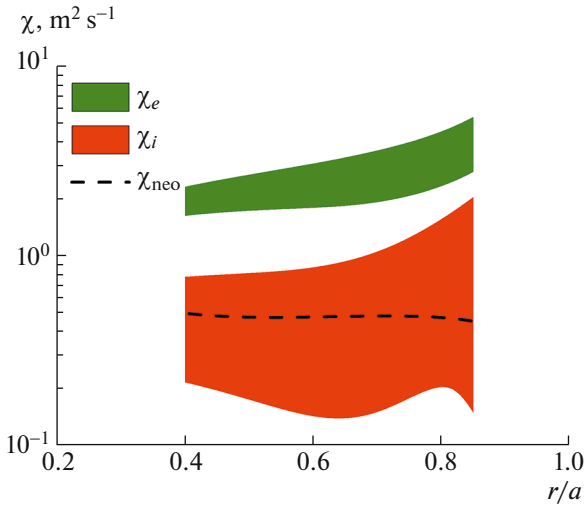

Fig. 17. Radial distributions of electron (green) and ion (red) effective thermal conductivity in comparison with neoclassical ion thermal conductivity calculated using NCLASS code (dashed line) for plasma of Globus-M2 with $B_T = 0.9$ T, $I_p = 0.35$ MA, and $P_{NBI} = 0.7$ MW.

occurs due to the radiation loss, which can reach half the plasma heating power [37]. Under these assumptions, we obtain $\chi_e = 1.5–3$ m^2 s^{-1}. The plasma energy balance was also analyzed with higher accuracy performing simulations using the ASTRA code [34]. The resulting radial distributions of the effective electron and ion thermal diffusivities are shown in Fig. 17. It can be seen in the figure that the thermal diffusivities of electrons and ions, obtained in simulations and using the approximate formula, agree satisfactorily. The thermal diffusivity of ions calculated using the NCLASS code is approximately 0.5 m^2 s^{-1}, which falls in the range of the χ_i coefficients obtained when simulating the experimental data. We note that, in contrast to the experiments on plasma heating with the help of one beam, described in Section 3, the ion thermal insulation observed in the two-beam experiment is much better, and the heat transport is close to the neoclassical one. This makes it possible to reach temperatures close to those required for fusion reaction even at the compact facility such as the Globus-M2 tokamak.

5. CONCLUSIONS

The plasma heating using NBI was studied at the Globus M2 tokamak. In experiments using the beam with the particle energies of 45 keV and beam power of 0.75 MW, at the plasma current $I_p = 0.4$ MA and toroidal magnetic field $B_T = 0.8$ T at the axis of the vacuum chamber, the following results were obtained. At the mean electron density exceeding 3×10^{19} m^{-3}, the neutral beam injection results in considerable heating of plasma electrons. According to the Thomson scattering diagnostics, the electron temperature is almost independent of the electron density. Thermal energy of electrons linearly increases with increasing density, while in the OH regime (at the same current I_p and field B_T), the electron temperature decreases with increasing density. This results in saturation of the dependence of the W_e plasma energy stored in the electron component on the plasma density n_e. At high plasma density ($n_e > 7 \times 10^{19}$ m^{-3}), the electron temperature increases by 1.8 times, as compared to the OH regime. As the n_e plasma density increases, the power of ion heating increases too and ion heat transport becomes important for the energy balance. It was expected that in the case of the neoclassical nature of heat loss through the ion channel, the energy confinement time would reach 15 ms at the density $n_e = 7 \times 10^{19}$ m^{-3}. However, the joint analysis of the results of diamagnetic measurements and the Thomson scattering measurements of the electron temperature and density profiles indicates the presence of anomalous heat loss through the ion channel at high plasma densities. This results in saturation of the $\tau_E(n_e)$ dependence at plasma densities higher than 6×10^{19} m^{-3}; the level of saturation is $\tau_E \approx 10–11$ ms.

In the studies, the two-beam-injection scenario was used too: at the toroidal magnetic field increased to 0.9 T, the first and second beams were injected in the stages of current rise and current plateau, respectively. The use of this scenario radically changes the efficiency of plasma heating. The experiments have shown the possibility of obtaining the stable hot ion mode in a wide range of mean plasma densities: $(1.6–16) \times 10^{19}$ m^{-3}. The ion temperatures measured using the diagnostics of charge exchange recombination spectroscopy and neutral particle analyzer reached 4 keV, which is 2.5 times higher than the electron temperature. It became possible to obtain such parameters due to good thermal insulation of electrons and ions, but it was possible in a limited range of plasma densities. At the same time, the transport analysis showed that the ion thermal diffusivity is less than 1 m^2 s^{-1}, and this is in satisfactory agreement with the neoclassical theory.

We note that in the hot ion mode, the collisionality ($\nu^* \sim Z_{eff} n_e / T^2$) was approximately 0.005. To date, this is the lowest ν^* collisionality observed at the Globus-M2 tokamak. The ratio of the gas-kinetic pressure of plasma to the toroidal magnetic field pressure (β_T) reached 0.04–0.05. Gyrokinetic simulations performed for the Globus-M2 tokamak using the GENE code predicted the development of the ITG instability even under conditions of 2–4 times higher collisionalities [15]. Despite the conditions favorable for destabilization of the ITG instability, no considerable anomalous ion heat transport was observed. The reason for this may be the inhomogeneity of plasma rotation,

which results in the disturbance of turbulent structure and a decrease in heat transport across the magnetic field. In the hot ion mode, using the CXRS diagnostics, the strong toroidal rotation of plasma was measured with the velocity reaching 190 km/s in the paraxial region of the plasma column. Apparently, this makes possible the transition to the hot ion mode.

The results presented in this work show the possibility of reaching high ion temperatures in the compact facility with relatively weak toroidal magnetic field. In the experiments, due to the good thermal insulation of the ions, the ion temperatures were reached close to thermonuclear ones. In this case, for the plasma of the Globus-M2 tokamak, the product of characteristic parameters ($n_e\tau_E$) is as yet two orders of magnitude lower than that required for the ignition of the self-sustained fusion reaction. However, bearing in mind that in spherical tokamaks, the dependence of the confinement time on the magnetic field and major plasma radius R is favorable [5, 15], we can assume that in a compact facility ($R = 0.8$ m) with the strong magnetic field (of approximately 5 T), it can be possible to reach the ignition conditions. On the way to achieving this goal, the technical difficulties associated with creating and operating a compact fusion device will be the main obstacles.

ACKNOWLEDGMENTS

The experiments were carried out at the Unique Scientific Installation "Globus-M Spherical Tokamak," which is a part of the Federal Center for the Collective Use of Scientific Equipment "Materials Science and Diagnostics in Advanced Technologies."

The calculations of plasma heating power were performed using the computing resources of the Supercomputer Center "Polytechnic" of Peter the Great St. Petersburg Polytechnic University (http://www.spbstu.ru).

FUNDING

Experiments on plasma heating by two beams at $B_T = 0.9$ T (Subsection 4.1) were supported by the RF Ministry of Science and Higher Education under the State Contract no. 0034-2021-0001, and data processing and plasma energy balance simulations (Subsection 4.2) were supported by the RF Ministry of Science and Higher Education under the State Contract no. 0040-2019-0023. Analysis of plasma thermal insulation presented in Subsection 3.2 was supported by the Russian Science Foundation (project no. 17-72-20076).

CONFLICT OF INTEREST

The authors declare that they have no conflicts of interest.

OPEN ACCESS

REFERENCES

1. G. S. Kurskiev, N. N. Bakharev, V. V. Bulanin, F. V. Chernyshev, V. K. Gusev, N. A. Khromov, E. O. Kiselev, V. B. Minaev, I. V. Miroshnikov, E. E. Mukhin, M. I. Patrov, A. V. Petrov, Yu. V. Petrov, N. V. Sakharov, P. B. Shchegolev, et al., Nucl. Fusion **59**, 066032 (2019). https://doi.org/10.1088/1741-4326/ab15c5
2. G. S. Kurskiev, V. K. Gusev, N. V. Sakharov, I. M. Balachenkov, N. N. Bakharev, V. V. Bulanin, F. V. Chernyshev, A. A. Kavin, E. O. Kiselev, N. A. Khromov, V. B. Minaev, I. V. Miroshnikov, M. I. Patrov, A. V. Petrov, Yu. V. Petrov, et al., Nucl. Fusion **61**, 064001 (2021). https://doi.org/10.1088/1741-4326/abe08c
3. M. Valovič, R. Akers, G. Cunningham, L. Garzotti, B. Lloyd, D. Muir, A. Patel., D. Taylor, M. Turnyanskiy, M. Walsh, and the MAST team, Nucl. Fusion **49**, 075016 (2009). https://doi.org/10.1088/0029-5515/49/7/075016
4. S. M. Kaye, M. G. Bell, R. E. Bell, E. D. Fredrickson, B. P. LeBlanc, K. C. Lee, S. Lynch, and S. A. Sabbagh, Nucl. Fusion **46**, 848 (2006). https://doi.org/10.1088/0029-5515/46/10/002
5. S. M. Kaye, J. W. Connor, and C. M. Roach, Plasma Phys. Controlled Fusion **63**, 123001 (2021). https://doi.org/10.1088/1361-6587/ac2b38
6. S. M. Kaye, S. Gerhardt, W. Guttenfelder, R. Maingi, R. E. Bell, A. Diallo, B. P. LeBlanc, and M. Podesta, Nucl. Fusion **53**, 063005 (2013). https://doi.org/10.1088/0029-5515/53/6/063005
7. M. Valovič, R. Akers, M. de Bock, J. McCone, L. Garzotti, C. Michael, G. Naylor, A. Patel, C. M. Roach, R. Scannell, M. Turnyanskiy, M. Wisse, W. Guttenfelder, J. Candy, and the MAST team, Nucl. Fusion **51**, 073045 (2011). https://doi.org/10.1088/0029-5515/51/7/073045
8. E. J. Doyle, W. A. Houlberg, Y. Kamada, V. Mukhovatov, T. H. Osborne, A. Polevoi, G. Bateman, J. W. Connor, J. G. Cordey, T. Fujita, X. Garbet, T. S. Hahm, L. D. Horton, A. E. Hubbard, F. Imbeaux, et al., Nucl. Fusion **47**, S18 (2007). https://doi.org/10.1088/0029-5515/47/6/S02

9. F. van Wyk, E. G. Highcock, A. R. Field, C. M. Roach, A. A. Schekochihin, F. I. Parra, and W. Dorland, Plasma Phys. Controlled Fusion **59**, 114003 (2017). https://doi.org/10.1088/1361-6587/aa8484
10. A. Yu. Telnova, G. S. Kurskiev, I. V. Miroshnikov, N. V. Sakharov, E. O. Kiselev, M. M. Larionova, N. N. Bakharev, D. M. Larionova, V. K. Gusev, N. A. Khromov, V. B. Minaev, M. I. Patrov, Yu. V. Petrov, A. D. Sladkomedova, P. B. Shchegolev, et al., Plasma Phys. Controlled Fusion **62**, 045011 (2020). https://doi.org/10.1088/1361-6587/ab6da5
11. A. Yu. Tel'nova, I. V. Miroshnikov, M. M. Mitrankova, N. N. Bakharev, V. K. Gusev, N. S. Zhil'tsov, E. O. Kiselev, G. S. Kurskiev, V. B. Minaev, Yu. V. Petrov, N. V. Sakharov, P. B. Shchegolev, and E. A. Tukhmeneva, Tech. Phys. Lett. **47**, 470 (2021). https://doi.org/10.1134/S106378502105014X
12. A. A. Galeev and R. Z. Sagdeev, *Neoclassical Theory of Diffusion (Advances in Plasma Physics, Vol. 6)* (Wiley, New York, 1976), pp. 311–420.
13. V. K. Gusev, E. A. Azizov, A. B. Alekseev, A. F. Arneman, N. N. Bakharev, V. A. Belyakov, S. E. Bender, E. N. Bondarchuk, V. V. Bulanin, A. S. Bykov, F. V. Chernyshev, I. N. Chugunov, V. V. Dyachenko, O. G. Filatov, A. D. Iblyaminova, et al., Nucl. Fusion **53**, 093013 (2013). https://doi.org/10.1088/0029-5515/53/9/093013
14. E. O. Kiselev, N. N. Bakharev, V. V. Bulanin, V. K. Gusev, N. A. Khromov, G. S. Kurskiev, V. B. Minaev, I. V. Miroshnikov, M. I. Patrov, A. V. Petrov, Yu. V. Petrov, N. V. Sakharov, P. B. Schegolev, A. Yu. Telnova, V. A. Tokarev, et al., J. Phys.: Conf. Ser. **1383**, 012003 (2019). https://doi.org/10.1088/1742-6596/1383/1/012003
15. G. S. Kurskiev, V. K. Gusev, N. V. Sakharov, Yu. V. Petrov, N. N. Bakharev, I. M. Balachenkov, A. N. Bazhenov, F. V. Chernyshev, N. A. Khromov, E. O. Kiselev, S. V. Krikunov, V. B. Minaev, I. V. Miroshnikov, A. N. Novokhatskii, N. S. Zhiltsov, et al., Nucl. Fusion **62**, 016011 (2022). https://doi.org/10.1088/1741-4326/ac38c9
16. A. Yu. Telnova, V. B. Minaev, P. B. Shchegolev, N. N. Bakharev, I. V. Shikhovtsev, and V. I. Varfolomeev, J. Phys.: Conf. Ser. **1400**, 077015 (2019). https://doi.org/10.1088/1742-6596/1400/7/077015
17. V. K. Gusev, A. V. Dech, L. A. Esipov, V. B. Minaev, A. G. Barsukov, G. B. Igon'kina, V. V. Kuznetsov, A. A. Panasenkov, M. M. Sokolov, G. N. Tilinin, A. V. Lupin, and V. K. Markov, Tech. Phys. **52**, 1127 (2007). https://doi.org/10.1134/S1063784207090058
18. V. B. Minaev, V. K. Gusev, N. V. Sakharov, V. I. Varfolomeev, N. N. Bakharev, V. A. Belyakov, E. N. Bondarchuk, P. N. Brunkov, F. V. Chernyshev, V. I. Davydenko, V. V. Dyachenko, A. A. Kavin, S. A. Khitrov, N. A. Khromov, E. O. Kiselev, et al. Nucl. Fusion **57**, 066047 (2017). https://doi.org/10.1088/1741-4326/aa69e0
19. V. I. Vasiliev, Yu. A. Kostsov, K. M. Lobanov, L. P. Makarova, A. B. Mineev, V. K. Gusev, R. G. Levin, Yu. V. Petrov, and N. V. Sakharov, Nucl. Fusion **46**, 625 (2006). https://doi.org/10.1088/0029-5515/46/8/S08
20. N. V. Sakharov, A. V. Voronin, V. K. Gusev, A. A. Kavin, S. N. Kamenshchikov, K. M. Lobanov, V. B. Minaev, A. N. Novokhatskii, M. I. Patrov, Yu. V. Petrov, and P. B. Shchegolev, Plasma Phys. Rep. **41**, 997 (2015). https://doi.org/10.1134/S1063780X15120120
21. A. Yu. Tel'nova, V. B. Minaev, A. A. Panasenkov, and P. B. Shchegolev, Zh. Tekh. Fiz. **92** (4), 540 (2022). https://doi.org/10.21883/JTF.2022.04.52240.292-21
22. S. A. Galkin, A. A. Ivanov, S. Yu. Medvedev, and Yu. Yu. Poshekhonov, Nucl. Fusion **37**, 1455 (1997). https://doi.org/10.1088/0029-5515/37/10/I11
23. E. E. Tkachenko, N. V. Sakharov, and G. S. Kurskiev, in *The 21st International Spherical Torus Workshop, Beijing, 2022,* Book of Abstracts, p. 5.
24. G. S. Kurskiev, N. S. Zhiltsov, A. N. Koval', A. F. Kornev, A. M. Makarov, E. E. Mukhin, Yu. V. Petrov, N. V. Sakharov, V. A. Solovei, E. E. Tkachenko, S. Yu. Tolstyakov, and P. V. Chernakov, Pis'ma Zh. Tekh. Fiz. **47** (24), 41 (2021). https://doi.org/10.21883/PJTF.2021.24.51799.19019
25. N. S. Zhiltsov, Nucl. Fusion (in press).
26. G. F. Avdeeva, I. V. Miroshnikov, N. N. Bakharev, G. S. Kurskiev, M. I. Patrov, V. Yu. Sergeev, and P. B. Schegolev, J. Phys.: Conf. Ser. **666**, 012002 (2016). https://doi.org/10.1088/1742-6596/666/1/012002
27. M. M. Larionova, I. V. Miroshnikov, V. K. Gusev, V. B. Minaev, M. I. Patrov, Yu. V. Petrov, N. V. Sakharov, P. B. Schegolev, A. Yu. Telnova, and N. N. Bakharev, J. Phys.: Conf. Ser. **1400**, 077018 (2019). https://doi.org/10.1088/1742-6596/1400/7/077018
28. N. N. Bakharev, F. V. Chernyshev, V. K. Gusev, E. O. Kiselev, G. S. Kurskiev, M. M. Larionova, A. D. Melnik, V. B. Minaev, M. I. Mironov, I. V. Miroshnikov, Yu. V. Petrov, N. V. Sakharov, P. B. Shchegolev, O. M. Skrekel, A. Yu. Telnova, et al., Plasma Phys. Controlled Fusion **62**, 125010 (2020). https://doi.org/10.1088/1361-6587/abbe32
29. O. M. Skrekel, N. N. Bakharev, V. I. Varfolomeev, V. K. Gusev, M. V. Il'yasova, A. Yu. Telnova, E. M. Khilkevich, and A. E. Shevelev, Tech Phys. **92**, 12 (2021). https://doi.org/10.21883/TP.2022.01.52526.151-21
30. Yu. V. Petrov, V. K. Gusev, N. V. Sakharov, V. B. Minaev, V. I. Varfolomeev, V. V. Dyachenko, I. M. Balachenkov, N. N. Bakharev, E. N. Bondarchuk, V. V. Bulanin, F. V. Chernyshev, M. V. Iliasova, A. A. Kavin, E. M. Khilkevitch, N. A. Khromov, et al., Nucl. Fusion **62**, 042009 (2022). https://doi.org/10.1088/1741-4326/ac27c7
31. A. Pankin, D. McCune, R. Andre, G. Bateman, and A. Kritz, Comput. Phys. Commun. **159**, 157 (2004). https://doi.org/10.1016/j.cpc.2003.11.002
32. N. N. Bakharev, F. V. Chernyshev, P. R. Goncharov, V. K. Gusev, A. D. Iblyaminova, V. A. Kornev, G. S. Kurskiev, A. D. Melnik, V. B. Minaev, M. I. Mironov, M. I. Patrov, Yu. V. Petrov, N. V. Sakharov, P. B. Shchegolev, S. Yu. Tolstyakov, et al., Nucl. Fusion **55**, 043023 (2015). https://doi.org/10.1088/0029-5515/55/4/043023

33. W. W. Heidbrink, D. Liu, Y. Luo, E. Ruskov, and B. Geiger, Commun. Comput. Phys. **10**, 716 (2011). https://doi.org/10.4208/cicp.190810.080211a

34. G. Pereverzev and P. N. Yushmanov, Report No. 5/98 (Max-Plank Institute for Plasma Physics, Garching, 2002). http://w3.pppl.gov/~hammett/work/2009/Astra_ocr.pdf.

35. E. A. Tukhmeneva, S. Yu. Tolstyakov, G. S. Kurskiev, V. K. Gusev, V. B. Minaev, Yu. V. Petrov, N. V. Sakharov, A. Yu. Telnova, N. N. Bakharev, P. B. Shegolev, and E. O. Kiselev, Plasma Sci. Technol. **21**, 105104 (2019). https://doi.org/10.1088/2058-6272/ab305f

36. W. A. Houlberg, K. C. Shaing, S. P. Hirshman, and M. C. Zarnstorff, Phys. Plasmas **4**, 3230 (1997). https://doi.org/10.1063/1.872465

37. E. A. Tukhmeneva, N. N. Bakharev, V. I. Varfolomeev, V. K. Gusev, N. S. Zhil'tsov, E. O. Kiselev, G. S. Kurskiev, V. B. Minaev, Yu. V. Petrov, N. V. Sakharov, A. D. Sladkomedova, A. Yu. Tel'nova, S. Yu. Tolstyakov, and P. B. Shchegolev, Tech. Phys. Lett. **47**, 56 (2021). https://doi.org/10.1134/S1063785021010272

Translated by I. Grishina